The deacylase sirtuin 5 reduces malonylation in nonmitochondrial metabolic pathways in diabetic kidney disease

Judy Baek[1,2], Kelli Sas[1], Chenchen He[1], Viji Nair[1,3], William Giblin[4], Ayaka Inoki[5], Hongyu Zhang[1], Yang Yingbao[4], Jeffrey Hodgin[4], Robert G. Nelson[6], Frank C. Brosius III,[1,2,7], Matthias Kretzler[1,3], Paul M. Stemmer[8], David B. Lombard[4,9], and Subramaniam Pennathur[1,2,*]

From the [1]Department of Internal Medicine-Nephrology, [2]Department of Molecular and Integrative Physiology, [3]Department of Computational Medicine and Bioinformatics, and [4]Department of Pathology, University of Michigan, Ann Arbor, Michigan, USA; [5]Department of Biology, Johns Hopkins University, Baltimore Maryland, USA; [6]Chronic Kidney Disease Section, National Institute of Diabetes and Digestive and Kidney Diseases, Phoenix, Arizona, USA; [7]Department of Medicine, University of Arizona, Tucson, Arizona, USA; [8]Institute of Environmental Health Sciences, Wayne State University, Detroit, Michigan, USA; [9]Institute of Gerontology, University of Michigan, Ann Arbor, Michigan, USA

Reviewed by members of the JBC Editorial Board. Edited by Dennis Voelker

Early diabetic kidney disease (DKD) is marked by dramatic metabolic reprogramming due to nutrient excess, mitochondrial dysfunction, and increased renal energy requirements from hyperfiltration. We hypothesized that changes in metabolism in DKD may be regulated by Sirtuin 5 (SIRT5), a deacylase that removes posttranslational modifications derived from acyl-coenzyme A and has been demonstrated to regulate numerous metabolic pathways. We found decreased malonylation in the kidney cortex (~80% proximal tubules) of type 2 diabetic BKS *db/db* mice, associated with increased SIRT5 expression. We performed a proteomics analysis of malonylated peptides and found that proteins with significantly decreased malonylated lysines in the db/db cortex were enriched in nonmitochondrial metabolic pathways: glycolysis and peroxisomal fatty acid oxidation. To confirm relevance of these findings in human disease, we analyzed diabetic kidney transcriptomic data from a cohort of Southwestern American Indians, which revealed a tubulointerstitial-specific increase in Sirt5 expression. These data were further corroborated by immunofluorescence data of SIRT5 from nondiabetic and DKD cohorts. Furthermore, overexpression of SIRT5 in cultured human proximal tubules demonstrated increased aerobic glycolysis. Conversely, we observed reduced glycolysis with decreased SIRT5 expression. These findings suggest that SIRT5 may lead to differential nutrient partitioning and utilization in DKD. Taken together, our findings highlight a previously unrecognized role for SIRT5 in metabolic reprogramming in DKD.

Diabetic kidney disease (DKD) is the most prevalent cause of end-stage kidney disease in the United States, accounting for ~40% of all cases (1). Sodium–glucose cotransporter 2 (SGLT2) inhibitors were recently shown to provide significant protection against DKD progression that appears to be superior to that of renin–angiotensin (RAS) inhibitors, which were previously the mainstay of treatment (2–5). Although the mechanisms responsible for SGLT2 inhibitor protection are not known, the resultant reduction in glucose load into proximal tubules in patients with DKD suggests that preserving metabolic homeostasis of proximal tubules could represent an important part of this mechanism.

Proximal tubules undergo significant metabolic reprogramming in DKD. Under normal physiologic conditions, proximal tubules prefer to utilize fatty acids and glutamine for energy production and demonstrate low capacity for glucose utilization (6). In DKD, proximal tubules upregulate glucose utilization, potentially to supplement energy production that is diminished due to mitochondrial dysfunction. DKD is associated with increased urinary lactate production (7–10), and metabolomics studies of patient urine samples demonstrate that increase in tricarboxylic acid (TCA) cycle metabolites predict DKD progression in those with preserved renal function (11), whereas reduction in mitochondrial metabolites is observed with more advanced disease (12). Our previous *in vivo* metabolic flux study demonstrated that glucose utilization is increased in the kidney cortex (~80% proximal tubules by volume; Ref (13)) in BKS.Lepr$^{db/db}$ (*db/db*) mice, a pathophysiologically relevant model of DKD in type 2 diabetes (T2D) (11). This increase in glucose utilization occurred concurrently with increased pyruvate and palmitate catabolism and reduced mitochondrial ATP production capacity, supporting the idea that increased nutrient metabolism of many different substrates, and not only glucose, occurs in the kidney cortex in DKD to compensate for mitochondrial dysfunction.

In a normal physiological setting, glycolysis and fatty acid oxidation (FAO) are coordinated through the negative regulation of metabolic enzymes in each respective pathway by metabolic intermediates and products derived from the contralateral pathway. One mechanism through which this

* For correspondence: Subramaniam Pennathur, spennath@umich.edu.

occurs is protein posttranslational modifications (PTMs). The majority of PTMs are reversible, particularly protein acylations, and the necessary acyl-substrates are provided by acyl-CoAs (*i.e.*, acetyl-CoA, malonyl-CoA, succinyl-CoA, glutaryl-CoA) derived from nutrient metabolism (14). Excessive accumulation of these modifications that ultimately perturb protein function, a phenomenon described as "carbon-stress," may occur in diabetes and obesity at faster rates due to the nutrient overload that leads to increased generation of acylating metabolites and contributes to metabolic dysfunction (15). The removal of these acylations is controlled by sirtuins, an NAD+-regulated class of lysine deacylases (14, 16–18). Previous studies of Sirtuin 1 and Sirtuin 3 found benefit with increased expression of these deacylases in DKD (19), consistent with the idea that excess accumulation of protein-acylations contributes to disease.

Malonylation, a reversible covalent lysine PTM derived from the substrate malonyl-CoA that can be removed by sirtuin 5 (SIRT5), has been found in many contexts to regulate glycolysis and gluconeogenesis (20–24). SIRT5 KO cultured hepatocytes exhibit increased malonylation of glycolytic enzymes, which results in decreased glucose flux that is attributed to a reduction in enzymatic activity of the modified enzymes (21). Therefore, we hypothesized that malonylation contributes to altered glucose flux in DKD. Indeed, studies of *db/db* mice and other various murine models of obesity identified increased malonylation of proteins in various tissues (22, 23, 25). In contrast to these previous findings, we found decreased levels of malonylation in the *db/db* kidney cortex with an increase in SIRT5 levels, suggesting a potential regulatory role of SIRT5 in DKD pathobiology. We identified the targets of decreased malonylation in the *db/db* cortex and demonstrate that SIRT5 may be a regulator of extramitochondrial ATP production in DKD.

Results

Malonylation is decreased in db/db kidney cortex due to upregulation in SIRT5 levels

To determine whether PTM levels are altered in the *db/db* kidney cortex, we assessed the levels of various PTMs and found that malonylation levels, in particular, were significantly decreased in the diabetic kidney cortex (Fig. 1, *A* and *B*). In contrast, succinylation levels were not significantly different between the *db/+* and *db/db* kidney cortex (Fig. 1, *C* and *D*), even though SIRT5 catalyzes removal of both malonyl and succinyl moieties. Cellular fractionation of the kidney cortex revealed that, while levels of malonylated proteins were visibly decreased in both mitochondrial and cytoplasmic compartments from the *db/db* mice (Fig. 2), the decrease in malonylation was only statistically significantly reduced in the cytoplasmic compartment of *db/db* mice (Fig. 2, *B* and *C*). To understand how malonylation levels were decreased in the *db/db* cortex, we examined levels of SIRT5 by immunoblot and

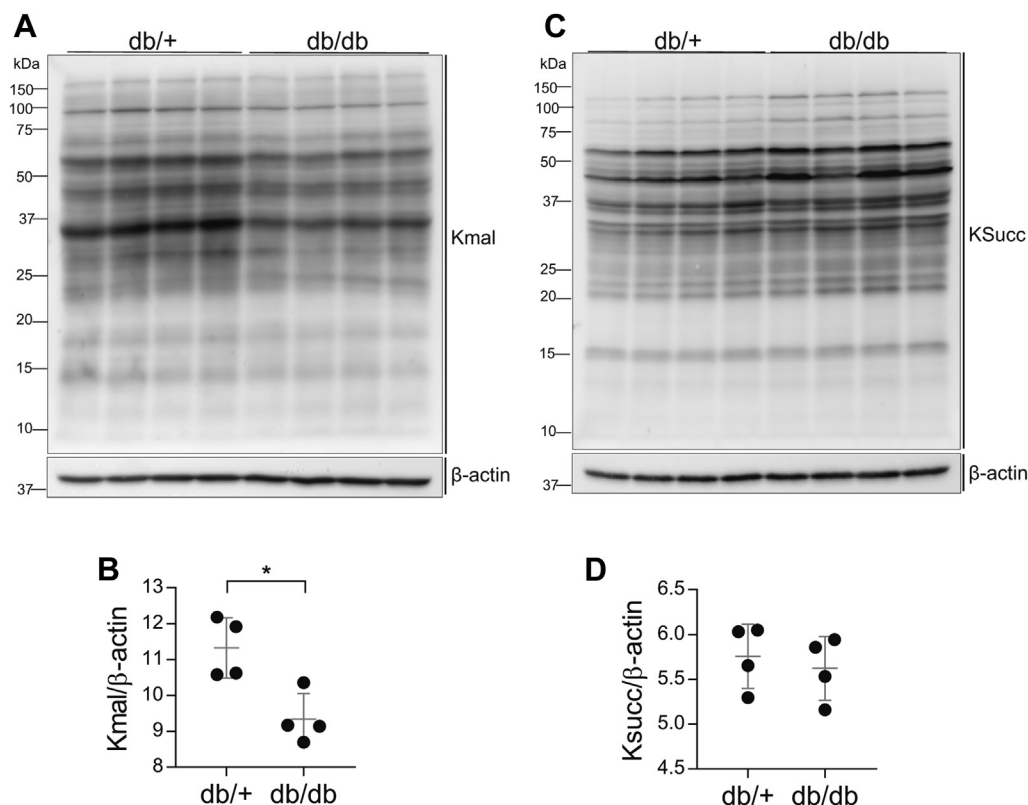**Figure 1. Malonylation is decreased in the *db/db* kidney cortex.** *A*, Western blot of db/+ and db/db cortex lysate probed for Kmal residues, n = 4. *B*, relative Western blot (*A*) signal of Kmal normalized to β-actin. *C*, Western blot of db/+ and db/db cortex lysate probed for Ksucc residues, n = 4. *D*, relative Western blot (*B*) signal of Ksucc normalized to β-actin. Student's *t* test, * = p < 0.05.
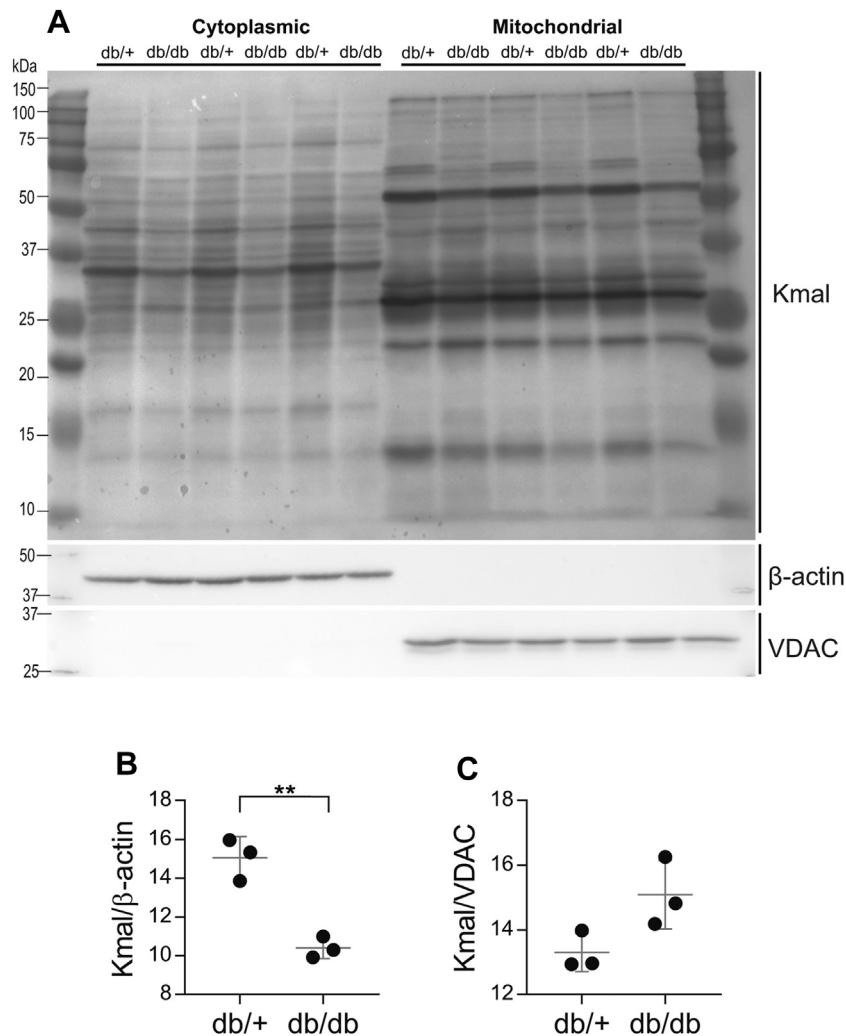
Figure 2. Compartment-specific reduction in protein malonylation levels. *A*, Western blot of proteins from the cytoplasmic and mitochondrial fractions db/+ and db/db cortex probed for Kmal residues, n = 3. *B*, relative Western blot signal intensities normalized against β-actin for Kmal in the cytosolic fraction. *C*, relative Western blot signal intensities normalized against voltage-dependent anion channel for Kmal in the mitochondrial fraction. Student's *t* test, ** = $p \le 0.01$.

quantitatively measured by LC-MS kidney cortex levels of malonyl-CoA, which serves as the acylating substrate for malonylation, and the NAD+/NADH ratio, as NAD+ serves as the cofactor for SIRT5 catalytic activity. Malonyl-CoA levels (Fig. 3A) and the NAD+/NADH (Fig. 3B) ratio were unchanged in the diabetic kidney cortex, whereas SIRT5 protein levels were significantly upregulated in the *db/db* cortex (Fig. 3, *C* and *D*), suggesting that SIRT5 activity, and not alterations in substrate or cofactor levels, drove the decrease in malonylation.

Malonylation is decreased specifically in proximal tubules in the db/db kidney

Proximal tubules comprise the majority of cells not only in the cortex but also in the entire kidney by mass (∼60% by mass) (26). To confirm that the changes in malonylation were primarily driven by proximal tubules, we conducted immunofluorescence analysis of malonylation residues in the *db/+* and *db/db* kidney cortex. Proximal tubules were identified with fluorescein-labeled Lotus Tetragonolobus Lectin, which

binds to the brush borders of proximal tubules. Malonylation-associated fluorescence was decreased in the *db/db* kidney proximal tubules (Fig. 4, *A* and *B*), consistent with the immunoblot data in Figure 1. Quantification of malonylation-associated fluorescence in other tubule segments (without brush borders) demonstrated no significant differences in malonylation levels between the control and diabetic kidneys (Fig. 4, *A* and *C*).

Immunoaffinity enriched proteomics for malonylated peptides identifies metabolic enzymatic pathways with decreased malonylation in the db/db kidney cortex

To identify differentially malonylated proteins in the *db/+* and *db/db* kidney cortex, we enriched for malonylated peptides with pan-antimalonyllysine antibodies and conducted label-free proteomics analysis (Supporting information 1). For relative quantification, we used Skyline MS1 filtering with normalization to a spiked heavy-labeled malonylated peptide standard, as previously published (21, 27). In total, we found 1719 malonylated peptides, of which 199 peptides exhibited
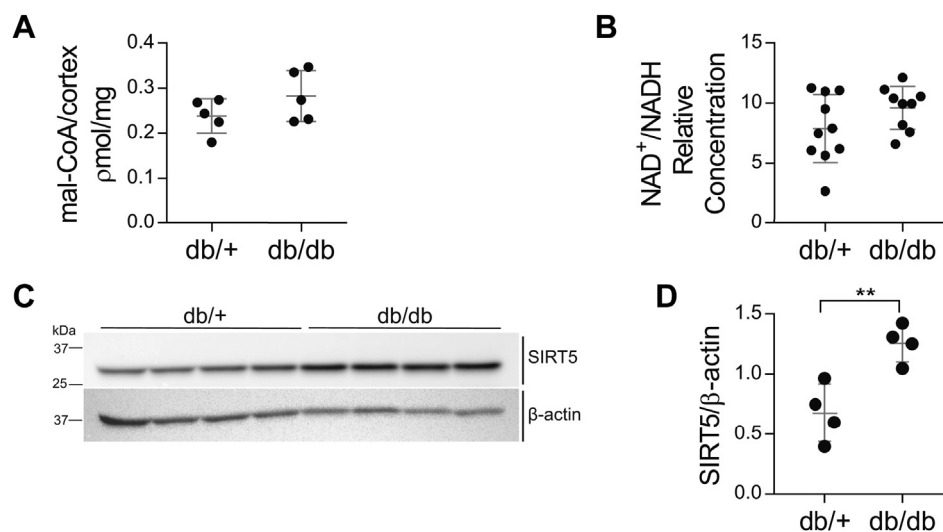
Figure 3. SIRT5 protein level is elevated in db/db kidney cortex. *A*, malonyl-CoA concentration normalized to tissue weight (pmol/mg) from db/+ and db/db kidney cortex, n = 5. *B*, NAD+/NADH concentration ratio from db/+ and db/db kidney cortex, n = 9–10. *C*, Western blot of db/+ and db/db cortex lysate probed for SIRT5, n = 4. *D*, relative Western blot (*A*) signal of SIRT5 normalized to β-actin. Student's *t* test, ** = $p \le 0.01$.

significantly higher levels of malonylation in the *db/db* cortex, whereas 259 peptides exhibited significantly lower levels of malonylation in the *db/db* cortex (Fig. 5*A*; Supporting information 2). Using DAVID functional enrichment analysis with KEGG pathway as the search database, pathways significantly enriched for peptides with significant downregulation of malonylation included "peroxisomes," "ribosomes," "pyruvate metabolism," "glycolysis/gluconeogenesis," and "glutathione metabolism" (Fig. 5*B*). Glycolytic targets in our assay with significantly decreased malonylation included aldolase A and B (Fig. 6*A*), and assessment of aldolase activity from *db/db* and *db/+* cortex demonstrated higher relative activity in the

diabetic conditions (Fig. 6*B*), consistent with previous findings. Peroxisomal targets were the most significantly enriched according to the functional enrichment analysis. Examination of the individual members demonstrated many of the proteins with decreased malonylation were involved in peroxisomal FAO (Fig. 7).

Peroxisomal fatty acid oxidation is increased in the db/db kidney cortex

Given the enrichment of peroxisomal targets, especially involved in FAO, we sought out to assess the relative rates of peroxisomal FAO in the *db/db* and *db/+* kidneys. We
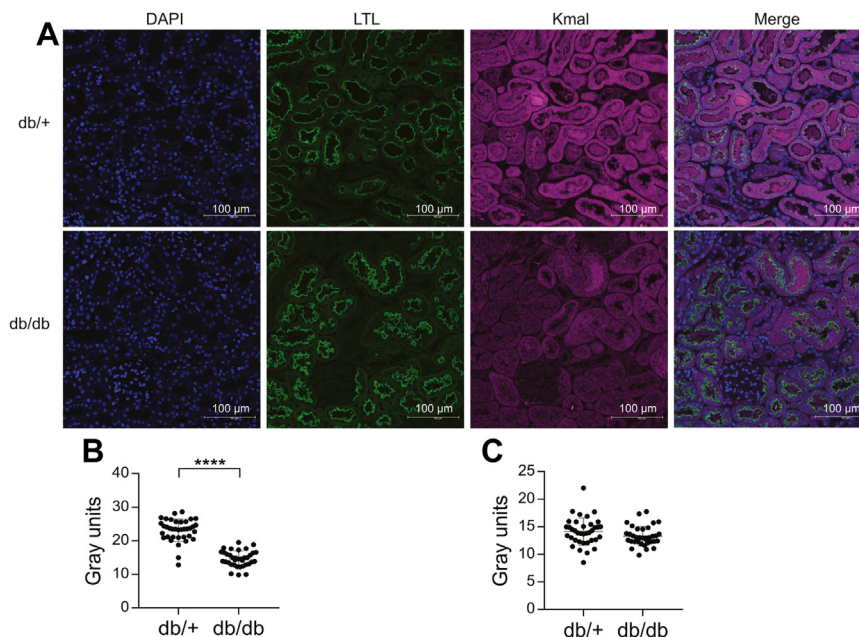
Figure 4. Immunofluorescence of Kmal residues in db/db and db/+ cortex. *A*, immunofluorescence of db/db and db/+ cortex with DAPI for nuclear stain, lotus tetragonolobus lectin (LTL) for proximal tubular brush border stain, and Kmal for malonylated residues. *B*, semiquantitation of fluorescence associated with Kmal residues in proximal tubules, *n* = 4. *C*, semiquantitation of fluorescence associated with Kmal residues in nonproximal tubules, *n* = 4. Student's *t* test, **** = $p \le 0.0001$.
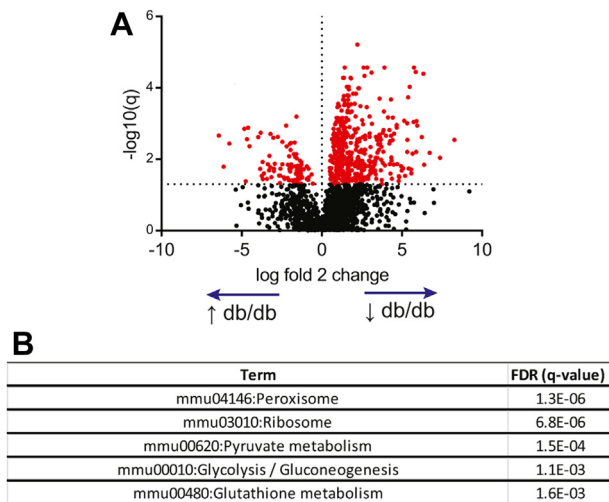
Figure 5. Immunoaffinity enriched proteomics for malonylation. *A,* volcano plot of malonylated peptides identified in the proteomics study. Peptides that were above the false discovery rate cutoff of 0.05 are highlighted in *red. B,* list of top metabolic pathways with decreased malonylated proteins in db/db kidney cortex obtained with DAVID functional annotation.

| Term	FDR (q-value)
mmu04146:Peroxisome	1.3E-06
mmu03010:Ribosome	6.8E-06
mmu00620:Pyruvate metabolism	1.5E-04
mmu00010:Glycolysis / Gluconeogenesis	1.1E-03
mmu00480:Glutathione metabolism	1.6E-03

employed a modified protocol from previous studies; instead of C^{14} palmitic acid, we used isotopically labeled $_{16}C^{13}$-palmitic acid as the substrate (28, 29). We utilized Etomoxir to inhibit mitochondrial FAO to study peroxisomal FAO exclusively (30). We monitored the first two resulting products of
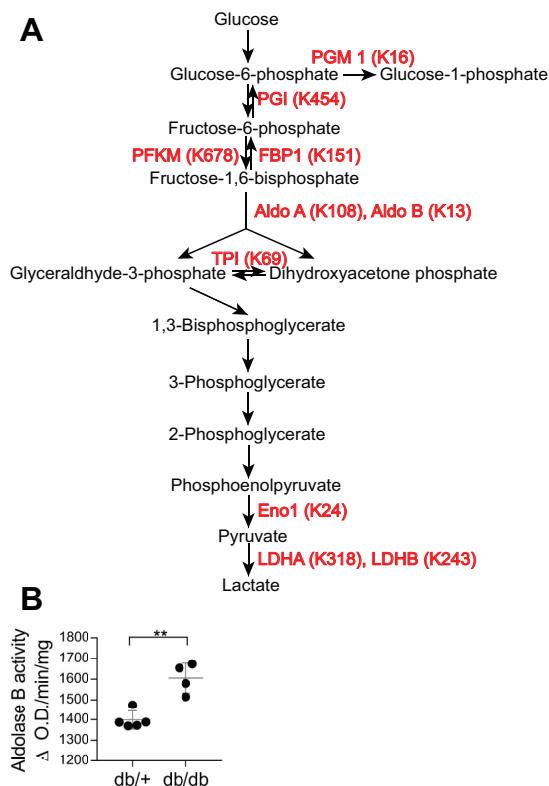

Figure 6. Proteins in glycolysis/gluconeogenesis with significantly reduced malonylation levels in the diabetic db/db cortex. *A,* protein names and their malonylated lysines that are significantly decreased in db/db cortex are denoted on the pathway in *red. B,* relative Aldolase *A* and *B* activity in the db/+ and db/db cortex, n = 3. Student's *t* test, ** = *p* ≤ 0.01.

$_{16}C^{13}$-palmitic acid oxidation, $_{12}C^{13}$-lauric acid and $_{14}C^{13}$-myristic acid, by mass spectrometry to determine the relative rates of peroxisomal FAO in freshly isolated *db/+* and *db/db* kidney cortex as described in Methods. Our analysis demonstrated that peroxisomal FAO of palmitate is enhanced in diabetic kidney cortex as assessed by the higher relative percent labeling of $_{12}C^{13}$-lauric acid and $_{14}C^{13}$-myristic acid (Fig. 8, *A* and *B*). As peroxisomal FAO enzymes were significantly demalonylated in the *db/db* cortex, our study suggests that reduction in malonylation may contribute to increased peroxisomal FAO.

SIRT5 expression is elevated in the tubulointerstitium of diabetic human kidney

To assess whether elevated SIRT5 levels are also observed in human DKD, we compared SIRT5 transcript levels derived from kidney biopsies of age-matched healthy control living donors (LD, n = 31) and Southwestern Native American patients with T2D with DKD (n = 77; Supporting information 3). The healthy control biopsies were obtained after perfusion pretransplant in individuals with normal kidney function, absence of proteinuria and normal blood pressure. The healthy control group had a higher percentage of males (51% *versus* 29%; *p* = 0.027) and was racially heterogenous compared with the Southwestern Native American T2D subjects. SIRT5 transcript levels derived from the glomerular compartment of the kidney were unchanged between the two groups, whereas SIRT5 transcript levels from the tubulointerstitial compartment were elevated, suggesting a tubulointerstitial-specific increase in SIRT5 in patients with T2D with DKD (Fig. 9). To directly assess for SIRT5 protein expression levels, we probed for SIRT5 in human kidney biopsies of nondiabetic and diabetic patients with established DKD derived from the University of Michigan Department of Pathology archives. Clinical and demographic data are displayed in Supporting information 4. Immunofluorescence analysis demonstrated significantly elevated SIRT5 levels in proximal tubules from diabetic kidneys (Fig. 10). In the nonproximal tubules, the difference in expression was not significant. These data are consistent with our RNA-Seq data from the Southwestern Native American cohort. Of note, Kmal levels by immunofluorescence were not significantly different between the diabetic and nondiabetic patients (Supporting information 5). This likely due to the fact that malonylation is a dynamic modification and can be influenced by timing of food intake (fed *versus* fasting) and dietary composition (caloric density and macronutrient composition). We suspect this issue could, in part, account for lack of changes observed in malonylation levels in diabetic kidney biopsies (21). Further studies need to be performed to better assess malonylation in human tissues as it is a dynamic PTM.

SIRT5 increases glucose flux into glycolysis in HK-2 cells in both low and high glucose conditions

Increased SIRT5 expression is associated with increased glucose flux in multiple contexts. To ascertain the role of
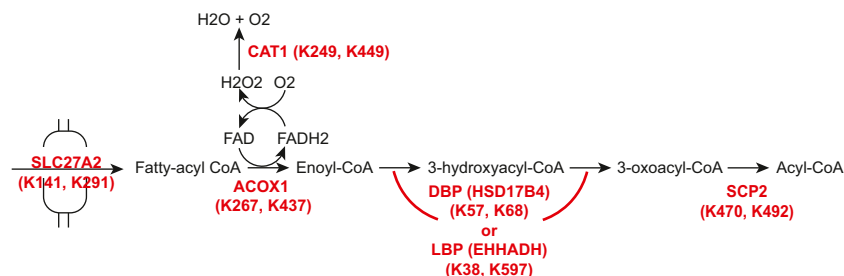
Figure 7. Proteins in peroxisomal fatty acid oxidation pathway with significantly reduced malonylation levels in the diabetic db/db cortex. Protein names and their malonylated lysines that are significantly decreased in the db/db cortex are denoted on the pathway in *red*.

SIRT5 in glucose metabolism in proximal tubules, we either overexpressed SIRT5 with lentiviral vector or knocked down SIRT5 with siRNA in a human proximal tubule cell line (HK-2) (Fig. 11A). We then supplemented the cell culture medium with 5 mM (low) or 25 mM (high) of $^{13}C_6$-glucose and allowed cells to metabolize the labeled glucose for 20 min or 4 h. Glycolytic and TCA cycle metabolites were then analyzed on a quadrupole time-of-flight mass spectrometer and relative abundances for isotopologues due to $^{13}C_6$-glucose catabolism were quantified. We found that overexpression of SIRT5 in HK-2 led to increased labeling of glycolytic metabolites such as pyruvate and DHAP (M + 3; Fig. 11, B and C) but decreased labeling of TCA cycle intermediates such as fumarate and citrate (M + 2; Fig. 11, D and E) in low glucose conditions. Glycolysis was enhanced with SIRT5 overexpression in high glucose as well (Fig. 12, A and B) but resulted in increased labeling of TCA cycle metabolites (Fig. 12, C and D).

Figure 8. Peroxisomal fatty acid oxidation in db/+ and db/db cortex. *A*, percentage of labeled $_{12}C^{13}$-lauric acid normalized to tissue weight (kidney cortex) as a product of peroxisomal fatty acid oxidation of $_{16}C^{13}$-palmitate. *B*, percentage of labeled $_{14}C^{13}$-myristic acid normalized to tissue weight (kidney cortex) as a product of peroxisomal fatty acid oxidation of $_{16}C^{13}$-palmitate. Student's *t* test, * = $p < 0.05$.

In contrast, SIRT5 knockdown (Fig. 13, A and B) led to decreased labeling of glycolytic intermediates such as lactate and pyruvate (M + 3; Fig. 13, C and D) but increased labeling of TCA cycle intermediates such as α-ketoglutarate and citrate/isocitrate (M + 2; Fig. 13, E and F), suggesting increased glucose-derived intermediate entry into the TCA cycle. These findings were also observed in HK-2 cells in high glucose conditions (Fig. 14). We interpret these findings to mean that SIRT5 increases lactate production and reduces pyruvate entry into mitochondria; indeed, previous studies have demonstrated that SIRT5 decreased activity of pyruvate dehydrogenase through desuccinylation (31). Decreased SIRT5 levels led to increased glucose metabolism through the mitochondria despite overall decreased levels of glucose flux into glycolysis.

Discussion

We found decreased malonylation in proximal tubules of *db/db* mice that is likely mediated by increased SIRT5 protein levels. Proteomic analysis of malonylated peptides from *db/db* and *db/+* kidney cortex demonstrated that proteins with significantly decreased malonylation were enriched in glycolysis/gluconeogenesis and peroxisomes, consistent with the fractionation data that demonstrate a reduction in malonylation levels specifically in the cytosol of the *db/db* cortex cytosol.

Overexpression of SIRT5 in HK-2 cells was associated with increased glucose utilization but reduced glucose-derived pyruvate shunting into TCA cycle metabolites in low glucose conditions. In high glucose, SIRT5 overexpression increased labeling of glycolytic and TCA cycle metabolites, potentially due to higher amount of pyruvate production in high glucose conditions, overcoming the inhibition of pyruvate shunting to TCA cycle seen in low glucose conditions. Reduction of SIRT5 levels in HK-2 cells was associated with the converse in both low and high glucose, suggesting that SIRT5 contributes to aerobic glycolysis and its reduction leads to increased pyruvate transfer to the TCA cycle.

Our findings support the hypothesis that the decreased malonylation observed in the *db/db* kidney cortex results in increased glucose flux observed from our *in vivo* flux studies (11). Previous studies in cultured hepatocytes (21) and chondrocytes (22) from Sirt5 KO mice found that increased malonylation results in a decreased glycolytic rate. Other studies have demonstrated a concentration-dependent
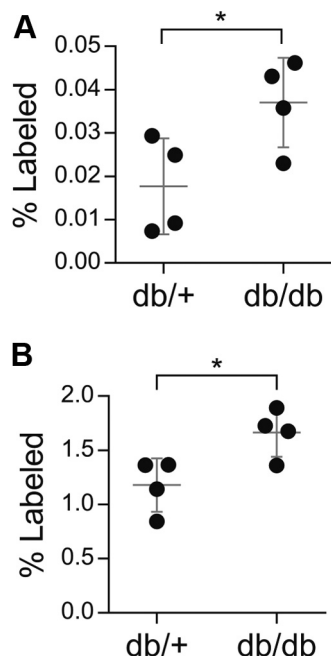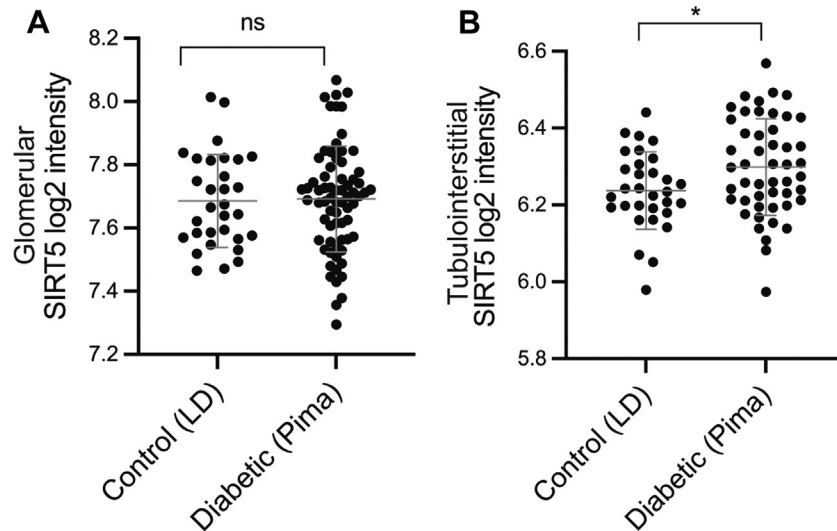
Figure 9. SIRT5 transcript levels from kidney biopsies of living donor (LD; control) volunteers and diabetic Southwestern Native Americans (Pima). *A*, glomerular SIRT5 transcript levels between LD and Pima kidney biopsies. *B*, tubulointerstitial SIRT5 transcript levels between LD and Pima kidney biopsies. Student's *t* test, ns = not significant, * = $p < 0.05$.

response to glucose utilization; SIRT5 overexpression in HEK293 led to increased glycolysis but only under high glucose (25 mM) conditions and not normoglycemic conditions (5 mM) (32). Our studies with the HK-2 cells demonstrated increased glycolysis with SIRT5 overexpression regardless of glucose levels but found a concentration-dependent response with regards to the TCA cycle. These data suggest that SIRT5 may have differential roles in metabolic regulation in normoglycemic and hyperglycemic conditions.

From our proteomics analysis we identified that the peroxisome is potentially regulated by malonylation. Peroxisomes contain >50 enzymes and catalyze numerous processes including oxidative stress defense, FAO, glyoxylate metabolism, and lipid and cholesterol synthesis (33). Recent studies have demonstrated that peroxisomes, which are particularly enriched in the kidney, play important role in tubular metabolism and physiology. A particular peroxisomal FAO protein of importance is Enoyl-CoA Hydratase and 3-Hydroxyacyl CoA Dehydrogenase (EHHADH), which catalyzes the second
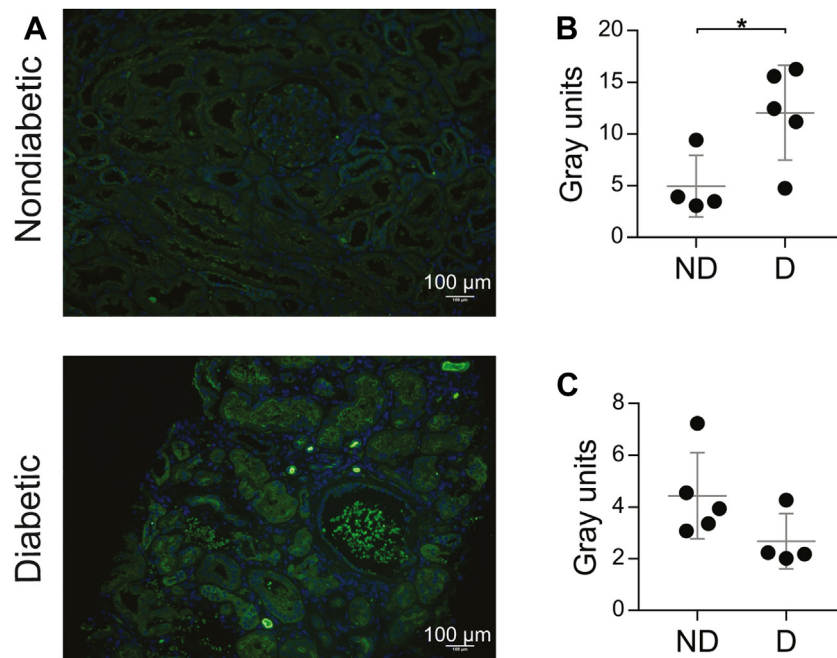
Figure 10. SIRT5 protein expression in human kidney biopsies. *A*, immunofluorescence images of diabetic (D) and nondiabetic (ND) human kidney biopsies. *Blue*, DAPI; *green*, SIRT5. *B*, semiquantitation of fluorescence associated with SIRT5 protein expression in proximal tubules, n = 4, 5. *C*, semiquantitation of fluorescence associated with SIRT5 protein expression in nonproximal tubules, n = 4, 5. Student's *t* test, * = $p < 0.05$.

Figure 11. Overexpression of SIRT5 in HK-2 cells in low glucose. *A*, Western blot of SIRT5 in HK-2 cells for wildtype (WT) and overexpression (OE) conditions. All graphs are expressed as % $_{13}$C labeled isotopologue of total metabolite: *B*, M + 3 pyruvate, n = 3. *C*, M + 3 dihydroxyacetone phosphate (DHAP) n = 3. *D*, M + 2 fumarate % labeled, n = 3. *E*, M + 2 citrate % labeled, n = 3. Student's *t* test, * = $p < 0.05$, ** = $p \leq 0.01$.

Figure 12. Overexpression of SIRT5 in HK-2 cells in high glucose. All graphs are expressed as % $_{13}$C labeled isotopologue of total metabolite: *A*, M + 3 pyruvate isotopologue levels represented by % total pyruvate level, n = 5, 6. *B*, M + 3 Lactate, n = 5, 6. *C*, M + 2 succinate % labeled, n = 5, 6. *D*, M + 2 citrate % labeled, n = 5, 6. Student's *t* test, * = $p < 0.05$, ** = $p \leq 0.01$.
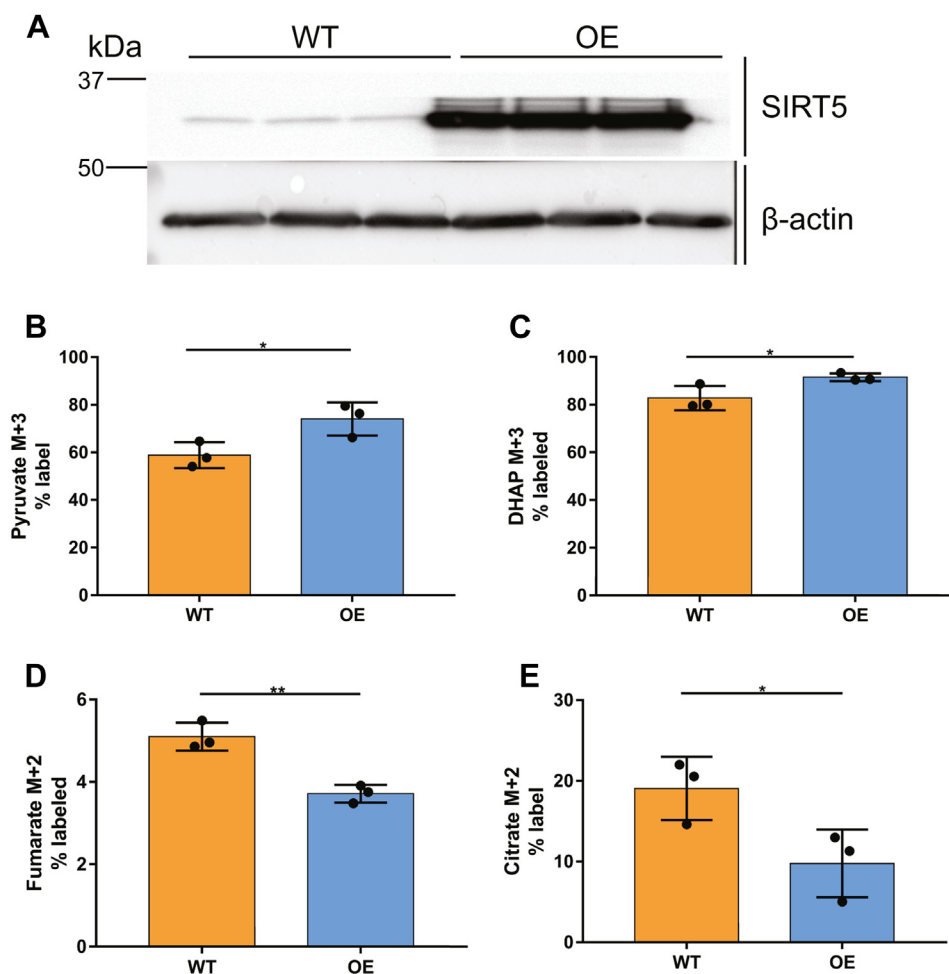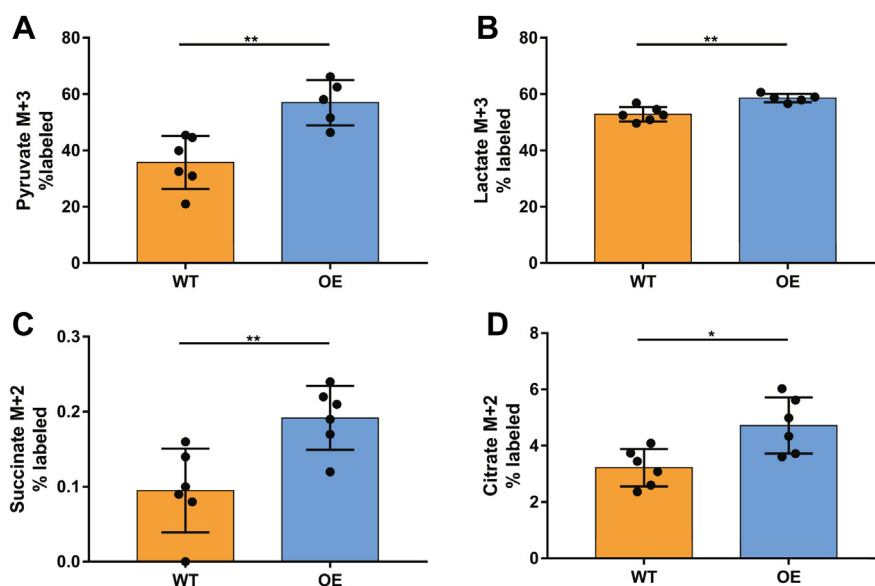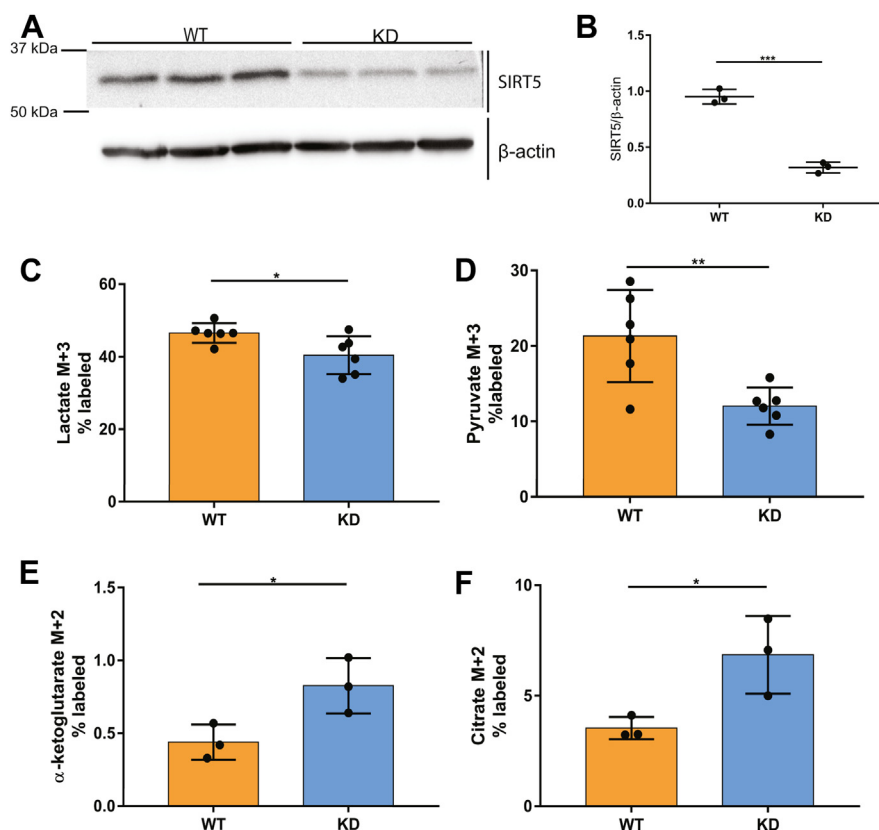
Figure 13. Knockdown of SIRT5 in HK-2 cells in low glucose. *A*, Western blot of SIRT5 in HK-2 cells for wildtype (WT) and knockdown (KD) conditions. All graphs are expressed as % $_{13}$C labeled isotopologue of total metabolite: *B*, relative band intensities of SIRT5 normalized to actin. *C*, M + 3 lactate % labeled, n = 6. *D*, M + 2 pyruvate % labeled, n = 6. *D*, M + 2 α-ketoglutarate % labeled, n = 3. *F*, M + 2 citrate % labeled, n = 3. Student's *t* test, * = $p < 0.05$, ** = $p \leq 0.01$, *** = $p \leq 0.001$.

and third reactions in peroxisomal β-oxidation. A recent study of global EHHADH KO mice demonstrated renal hypertrophy with mild glomerular filtration rate reduction and evidence of proximal tubular injury in male mice, but not female or orchiectomized EHHADH KO male mice (34). From our proteomics data, we found that the peroxisomal fatty acid machinery was prominently affected by decreased malonylation in the *db/db* cortex. In addition, our studies suggest that increased SIRT5 levels and decreased malonylation are associated with increased peroxisomal FAO, as evidenced by increased etomoxir-independent breakdown of palmitate in the *db/db* cortex *ex vivo*. However, there are some limitations
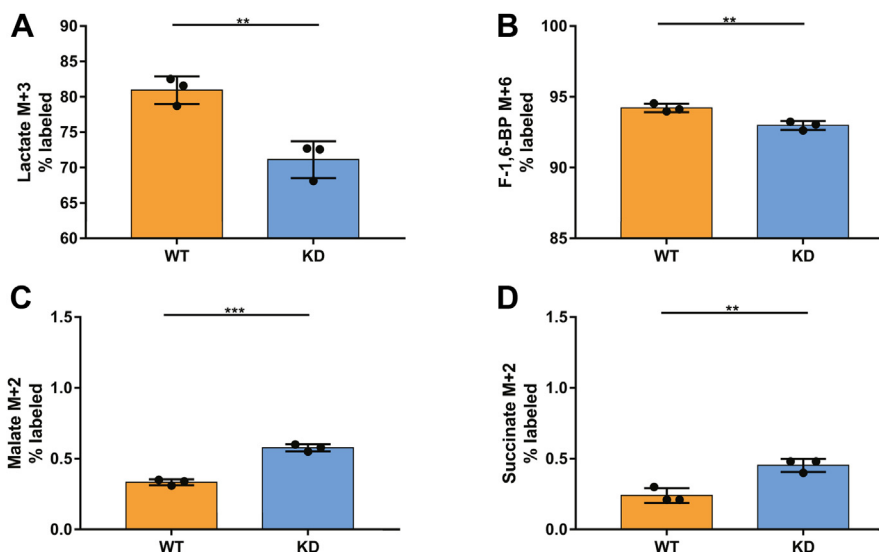

Figure 14. Knockdown of SIRT5 in HK-2 cells in high glucose. All graphs are expressed as % $_{13}$C labeled isotopologue of total metabolite: *A*, M + 3 lactate % labeled, *n* = 3. *B*, M + 6 F-1,6-BP % labeled, *n* = 3. *C*, M + 2 malate % labeled, *n* = 3. *D*, M + 2 succinate % labeled, *n* = 3. Student's *t* test, ** = $p \leq 0.01$, *** = $p \leq 0.001$.

to the peroxisomal studies. First, we measured peroxisomal activity *ex vivo*, which may not be replicated *in vivo*. Second, the association of malonylation to peroxisomal FAO is indirect in our study. Further studies in the future are needed to elucidate the direct role of malonylation in peroxisomal metabolism.

Other studies have also suggested that peroxisomal activity may be enhanced by SIRT5. SIRT5-mediated desuccinylation of ACOX1 is associated with decrease in its activity in hepatocytes (35). Chiba *et al.* found that SIRT5 KO mice are protected from different forms of acute kidney injury through a compensatory increase in peroxisomal FAO activity from the dampened baseline mitochondrial β-oxidation from the SIRT5 deficiency (29). The elevated peroxisomal FAO is thought to abrogate the loss in mitochondrial β-oxidation and dysfunction that occurs in acute kidney injury. On the other hand, acetylation of EHHADH is associated with an increase in its activity (36), and therefore reduced malonylation of EHHADH may conversely reduce its activity, although the charge states of the two modifications are different. The role of SIRT5 in peroxisomal metabolism in various kidney diseases remain to be elucidated.

The role of SIRT5 in diabetes and obesity is not well understood. Increased malonylation occurs in *db/db* and *ob/ob* mice livers (23), although high fat diet feeding in another study resulted in decreased malonylation (37), thought to be due to decreased malonyl-CoA production induced by increased lipid consumption. In *db/db* mice (22), the diet induced obesity mouse model, and proopiomelanocortin-deficient hyperphagic mice (25), increased malonylation occurs in chondrocytes. SIRT5 KO mice, which also display increased malonylation and succinylation in chondrocytes, exhibit increased joint dysfunction and an early osteoarthritic phenotype, correlating PTM accumulation with tissue dysfunction (25). Conversely, liver-specific SIRT5 overexpression in *ob/ob* mice results in decreased hepatic steatosis and hepatic triglyceride content (24), suggesting that decreased PTM levels improve tissue function. SIRT5 mice treated with streptozotocin to generate type 1 diabetes demonstrate no appreciable impact on diabetic retinopathy, but SIRT5 and SIRT3 double knockout diabetic mice demonstrate inner retinal dysfunction (38). Overall, current data suggest that hyperacylation and/or absence of SIRT5 levels contribute to tissue dysfunction, particularly in the context of metabolic diseases.

The increased level of SIRT5 we observed in the *db/db* cortex may therefore be an adaptive mechanism to reduce excess PTMs in DKD. Reduction in the malonylation of glycolytic enzymes, thereby increasing glucose flux through glycolysis, may prevent glucose shunting into secondary pathways, such as the polyol pathway and the methylglyoxal pathway, that generate toxic metabolic by-products. This mechanism of upregulating glycolysis may be particularly important in proximal tubules, which have little innate glycolytic capacity (6, 39–41), and thus benefit from any compensatory mechanisms to allow for proper glucose metabolism in DKD. SIRT5 also increases aerobic glycolysis, which generates energy without burdening the mitochondria. In addition, our data suggest that SIRT5 increases peroxisomal fatty acid oxidation, which may serve as an adjunct to mitochondrial lipid metabolism. Mitochondria from *db/db* mice cortex at 24 weeks of age demonstrate significantly elevated TCA cycle metabolites, suggesting mitochondrial overload in early DKD (11, 42), and increased activity of alternative energy-generating pathways may compensate for mitochondrial stress. On the other hand, increased SIRT5 levels in the kidney cortex may be detrimental. As SGLT2 inhibitors have demonstrated, decreasing glucose uptake by proximal tubules leads to disease amelioration (43). SIRT5 activity enhances glucose metabolism. Furthermore, aerobic glycolysis is associated with cellular hypertrophy and proliferation, fibroblast activation (44, 45), and epithelial–mesenchymal transition (46), which are all processes that contribute to DKD pathogenesis and progression.

We found that only malonylation, not succinylation, levels were decreased in the *db/db* cortex despite increased SIRT5 expression. In addition, the decrease in malonylation was compartment specific, occurring only in the cytoplasmic compartment at significant levels. A potential reason for this discrepancy is that succinate (11, 42) levels are significantly elevated in the *db/db* cortex and the rate of acylation may offset SIRT5 activity on mitochondrial succinylation. Another potential mechanism for the observed compartment specificity is that increased lactate production due to increased glycolysis and hypoxia in DKD may lead to increased NAD^+/NADH ratio in the cytosol, leading to increased SIRT5 activity specifically in the cytosol.

Further research is necessary to understand the role of SIRT5 in proximal tubular physiology in DKD. A limitation of our study is that tubular metabolism is difficult to recapitulate in immortalized cell culture or isolated tubular culture systems. HK-2 cells readily metabolize glucose, and therefore, it is difficult to ascertain whether our observations of SIRT5 expression and its role in glucose flux will translate to *in vivo* models. Future studies with SIRT5 mouse models of DKD will be needed to elucidate the role of SIRT5 in regulating metabolism in DKD.

Importantly, these models should examine knockdown and overexpression of SIRT 5 in a proximal tubule-specific manner to assess kidney-specific effects (as opposed to systemic effects on metabolism).

We found increased SIRT5 transcript levels in the tubulointerstitium of Southwestern Native Americans with T2D and DKD in comparison with nondiabetic living donors, consistent with the rodent studies. Immunofluorescence analysis of a small cohort of nondiabetic and DKD patient kidney biopsies demonstrated increased SIRT5 expression in the DKD group, further corroborating our mouse and Southwestern Native American data. Further assessment of whether SIRT5 levels are similarly elevated in other DKD cohorts, and whether the level of SIRT5 expression can predict disease progression, will aid in elucidating the importance of SIRT5 in DKD, thereby providing a rationale for therapeutically targeting Sirt5 (47).

Experimental procedures

Materials

$^{13}C_6$-glucose was purchased from Cambridge Isotope Labs Inc. Human kidney 2 (HK2) cells were purchased from American Type Culture Collection (ATCC CRL-2190). LC-MS-grade water, acetonitrile, chloroform, and methanol were obtained from Fisher Scientific. Malonyl-CoA and $^{13}C_3$-malonyl-CoA standards were purchased from Sigma-Aldrich. All other chemicals used in the study were purchased from Sigma-Aldrich unless otherwise indicated.

Cell culture

Cells were cultured in Dulbecco's modified Eagle's medium (DMEM)/F12 (11320033, Gibco; Thermo Fisher) supplemented with 1% pen/strep (Invitrogen), and 10% fetal bovine serum (FBS) (Corning) in humidified atmosphere of 5% CO_2 and 95% air at 37 °C.

Animals

Male BKS *db/db* mice (BKS.Lepr^db/db^/J) and littermate controls (*db/+*) were purchased from Jackson Labs at 12 weeks of age. Mice were housed in a climate-controlled, light-regulated facility with a 12:12 h light–dark cycle with water and chow ad libitum. At 24 weeks of age mice were harvested. Prior to sacrifice, mice were fasted for 4 h. The kidney was perfused with ice-cold PBS through the left ventricle and was dissected for the cortex region on ice. All samples were snap frozen and stored at −80 °C until analysis. The study was conducted according to the guidelines of the University of Michigan Committee on Use and Care of Animals.

Western blot

Cells and tissues were lysed in lysis buffer (2% SDS (w/v), 10% glycerol, 60 mM Tris-HCl pH 6.8) with 1 μM trichostatin A (Cayman), 20 mM nicotinamide, and 1× HALT protease inhibitor cocktail (Thermo Fisher). Samples were sonicated briefly on ice and centrifuged for 10 min at 17,000g. The supernatant was collected and protein concentration was determined with DC protein assay (Bio-Rad). The lysates were separated by SDS-PAGE and transferred to PVDF membranes. Signals were then visualized with Pierce ECL reagent (Thermo Fisher). Antibodies against Pan anti-malonyllysine (PTM-901) and Pan anti-succinyllysine (PTM-401) were purchased from PTM biolabs. Antibodies against SIRT5 (8782) and β-Actin (8H10D10) were purchased from Cell Signaling Technologies.

Kidney malonyl-lysine immunofluorescence

Kidney sections were fixed in 4% paraformaldehyde (Electron Microscopy Sciences) overnight at room temperature. Sections were paraffin embedded and cut into 3-μm sections for analysis. Slides were deparaffinized and incubated at 95 °C in antigen-unmasking solution (H-3300, Vector laboratories) for 2 h. Sections were blocked and permeabilized with 10% donkey serum and 0.5% Tween-20, respectively. Sections were incubated with pan anti-malonyllysine (PTM-901, PTM-

biolabs) and Lotus Tetragonolobus Lectin tagged with Fluorescein (FL-1321-2, Vector laboratories) overnight at 4 °C. Sections were then incubated with anti-rabbit IgG Alexa Fluor 647 (A-31573, Thermo Fisher). Resulting sections were visualized with Leica SP5 Confocal TCS Microscope. Semi-quantitation of immunofluorescence malonylation signals was analyzed with Leica Application Suite Lite 2.6.3.

Aldolase B activity assay

Activity assay was performed according to the manufacturer's directions with freshly perfused and dissected kidney cortex from *db/db* and *db/+* mice (ab196994; Abcam).

Kidney cortex fractionation

Freshly dissected cortex was stored in PBS on ice and homogenized with Teflon homogenizer in isolating medium (230 mM mannitol, 70 mM sucrose, 5 mM EGTA pH 8.0, 10 mM K-Hepes pH 7.4, 20 mM NAM, 1 μM trichostatin A, Protease inhibitor cocktail, 1 mM DTT). The homogenate was centrifuged at 1000g for 5 min at 4 °C. The supernatant was centrifuged at 10,000g for 10 min, and the resulting supernatant was collected as the cytosolic fraction. The pellet was resuspended in isolating medium and layered on 4 ml of 25% Percoll solution (GE healthcare; 90:10 Percoll: 2.5 M sucrose solution diluted 1:4 with 0.25 M Sucrose solution). The resuspension was centrifuged at 80,000g for 20 min at 4 °C. The resulting lower layer was collected as the mitochondrial fraction. The mitochondrial fraction was diluted with 30 ml of the isolating medium and centrifuged at 10,000g for 10 min. The resulting pellet was resuspended in 1× Laemmli buffer and sonicated before Western blot analysis. The cytosolic fraction was diluted 1:2 with 2× Laemmli buffer and sonicated before Western blot analysis. The samples were probed for malonyl-lysine residues as described.

Malonyl-CoA quantification

Malonyl-CoA was quantified by LC-MS as described ([48]). Briefly, tissue was sonicated in 10% trichloroacetic acid with $^{13}C_3$-malonyl-CoA. After sitting on ice, samples were centrifuged at 4500g for 5 min at 4 °C and the supernatant was extracted with 2:1 chloroform:methanol (*v/v*). The aqueous phase was dried under nitrogen and reconstituted in 10 mM ammonium acetate in water. For liquid chromatography (LC)/electrospray ionization (ESI)/tandem mass spectrometry (MS/MS) analysis, an Agilent 6410 triple quadruple MS system equipped with an Agilent 1200 LC system and ESI source was operated in positive ion mode. Malonyl-CoA (854.2 → 428.2 *m/z*) and $^{13}C_3$-malonyl-CoA (857.2 → 428.2 *m/z*) were detected in MRM mode, and relative peak areas were obtained and normalized to tissue weight.

NAD$^+$ and NADH quantification

Kidney cortex tissues were pulverized and sonicated in 80:20 acetonitrile:water (pH 9.0 with ammonium hydroxide) containing $^{13}C_6$-nicotinamide for internal standard. The homogenate was incubated on ice for 5 min and centrifuged for 10 min at

17,000g at 4 °C. LC-MS analysis was performed on an Agilent system consisting of a 1290 UPLC module coupled with a 6490 QqQ mass spectrometer (Agilent Technologies). Metabolites were separated on SeQuant ZIC-cHILIC (3 μm, 100 × 2.1 mm; Merck) with the following gradient: 0 to 2.5 min at 95% B, 2.5 to 8.5 min at 25% B, 8.5 to 8.6 min at 95% B, 8.6 to 12.6 min at 95% B. Solvent A was 50 mM ammonium acetate pH 8.0 in water, and solvent B was 100% acetonitrile. Column temperature was set at 30 °C, and flow rate was 0.3 ml/min. $^{13}C_6$-nicotinamide (129.1 → 85.1 *m/z*), NAD$^+$ (664.1 →136 *m/z*), and NADH (666.1 → 136 *m/z*) were monitored in MRM mode. Data were collected in positive mode.

Malonylation proteomics peptide preparation

Kidney cortex was homogenized in 5% SDS, 50 mM TEAB pH 7.55 supplemented with 1 uM trichostatin A and 20 mM nicotinamide using a Dounce homogenizer. Samples were sonicated for 20 s three times with 1 min rest on ice between cycles. Homogenates were spun at 17,500g for 20 min, and the supernatant was heated to 95 °C for 5 min to remove any residual protein activity. Protein concentration was measured with the DC protein assay kit. Protein, 25 mg, was treated with 5 mM DTT and incubated at 37 °C for 30 min with shaking. Samples were cooled and treated with 15 mM iodoacetamide at room temperature for 30 min with shaking in the dark. The alkylation reaction was quenched with 15 mM additional DTT. Samples were acidified by adding 12% phosphoric acid to 10% final volume of the sample, then 7 volumes of 90% methanol: TEAB solution, 10%, was added to precipitate the protein. Pellets were collected by centrifuging at 1000g for 2 min and resuspended in 50 mM TEAB with 0.1% deoxycholate. Trypsin was added at 1:50 trypsin to peptide ratio (wt/wt), and samples were digested at 37 °C with shaking for 24 h. The deoxycholate was precipitated by adding formic acid (FA) to a final concentration of 0.5% (v/v) and pelleted by centrifuging the samples at 3400g for 10 min. The supernatant containing the peptides was lyophilized for 24 h, then resuspended in 0.1% FA, and nonsoluble materials were removed by centrifugation. The supernatant was neutralized to pH 7.0 with ammonium hydroxide, and the peptide concentration was quantified with the Thermo Fischer peptide quantification kit.

Affinity enrichment of lysine malonylated peptides

Peptides, 9.5 mg, were affinity enriched for malonylated peptides by incubation with anti-malonyllysine antibody conjugated to Dynabeads in IAP buffer (50 mM Mops–NaOH, pH 7.2, 10 mM Na_2HPO_4, 50 mM NaCl) with 0.1% NP-40 at 4 °C for 24 h. Preselection, 250 ρg of heavy-labeled Malonyl-lysine (Kmal) peptide standards were added to each sample. The Kmal heavy-labeled peptide standard was synthesized by the University of Michigan peptide core. The synthesized sequence was as follows: H2N-TV*DGPSG(K/Malonyl)LWR-OH (V*: Valine $_{13}C^5$, $_{15}N$). Beads were washed twice with IAP + 0.1% 0.1% NP-40 buffer, twice with IAP, and once with water. Samples were eluted with 0.1% trifluoroacetic acid in water three times. Samples were desalted using desalting spin

column as per manufacturer's directions. Peptides were dried in a speed-vac for 1 h, and samples were stored at –80 °C until analysis.

Proteomics analysis

Peptides were dissolved in 25 μl 0.1% FA, and 10 μl of the sample was injected for analysis. Peptides were separated on reverse phase Thermo Scientific Acclaim PepMap 100: 75 μm × 2 cm (C18, 3 μm bead, 100 Å pore size) trap column and Thermo Scientific Acclaim PepMap C18, 2 μm particle size, RSLC 75 μm × 25 cm column. Data were acquired with Orbitrap QExactive coupled to Thermo Scientific Easy nLC-1000 UHPLC. Samples were run using a 90-min gradient from 5% "B" to 35% "B." Buffer "A" was 0.1% FA in water, and buffer "B" was 0.1% FA in acetonitrile. All data were acquired in positive mode with a lock mass of 445.12002 using data-dependent acquisition with a 15-s dynamic exclusion. MS1 data were acquired in profile mode at a resolution of 70,000 with a maximum time of 75 msec and a range of 350 to 1500 *m/z*. MS2 spectra were acquired in profile mode at a resolution of 15,000 and maximum integration time of 75 msec. The isolation window was 1.6 *m/z*, and the collision energy was 20.

Proteomics data analysis

RAW files for each sample were grouped and analyzed by MaxQuant (version 1.6.14.0). MS2 spectra were searched against the UniProt complete *Mus musculus* database concatenated with reverse decoy database (downloaded on August 20, 2020; http://www.uniprot.org) using the Andromeda search engine. Search parameters included up to three missed tryptic cleavages (Trypsin/P); 20 ppm match tolerance for MS1 ions and 0.02 Da for MS2 ions; and variable modifications for n-terminal acetylation, lysine acetylation, lysine malonylation, methionine oxidation, and fixed modification for cystine alkylation. A false discovery rate cutoff of 1% was used at the protein, peptide, and modification site for identification. MS1 quantitation was accomplished with Skyline v. 20.1.0.155. A spectral library of malonylated peptides was built with MaxQuant results. Digestion was set as Trypsin (KR/P) with three maxed missed cleavages. Peptides were filtered by minimum length of 8 and max length of 25. Peak areas were normalized to peak area of the spiked malonylated standard. Peptides with more than two missing data points in any one group were excluded from the analysis. Missing values were imputed with half-minimum of the lowest value in the group if all of the values in one group were lower than the lowest value in the other group. Otherwise, missing values were imputed with the k-NN method. Resulting values were normalized and Student's *t* test with FDR correction was conducted to identify peptides that were significantly altered between the two groups. Data processing was conducted with Metaboanalyst 5.0.

Lentivirus SIRT5 overexpression

Human *SIRT5* was cloned into the lentiviral plasmid, pLVX-EF1-IRES-mCherry, to generate SIRT5-overexpressing

lentivirus particles. The empty vector served as a negative control. Sequence integrity was confirmed by Sanger sequencing. Cells were confirmed for overexpression by sorting for mCherry-positive HK-2 cells. A total of 2×10^5 HK-2 cells were plated on 100-mm plates and allowed to attach overnight. Cells were treated with lentivirus with 8 μg/ml of polybrene at multiplicity of infection of 10 in DMEM/F12 with 10% FBS and no antibiotics. After 72 h, 5×10^5 cells were plated on six-well plates and allowed to attach overnight. Cells were serum fasted in DMEM/F12, 0.5% FBS, and 1% pen/strep for 24 h prior to labeling experiments.

SIRT5 siRNA knockdown

A total of 2×10^5 HK-2 cells were plated on six-well plates and allowed to attach overnight. Cells were treated with 100 ρmol of negative control or SIRT5 siRNA (AM4611, 19661; Thermo Fisher) with lipofectamine 3000 (Thermo Fisher) per manufacturer's instructions for 8 h. The medium was changed to DMEM/F12, 10% FBS, and 1% pen/strep for 16 h. Cells were then serum fasted in DMEM/F12, 0.5% FBS, and 1% pen/strep for 24 h prior to labeling experiments.

Glucose flux studies

A concentration of 5 mM (low) or 25 mM (high) $^{13}C_6$-glucose in DMEM, no glucose (Gibco 11966025, Thermo Fisher) was added to serum-fasted cells for 20 min and 4 h. After the designated time course, the medium was removed and cells were washed once with ice-cold 150 mM ammonium acetate in LC-MS grade water. Cells were then harvested with 200 μl of ice-cold methanol and frozen at −80 °C until sample preparation. For extraction, 200 μl of cold water was added to the cells and cells were scraped. The resulting homogenate was sonicated on ice for 10 s. A volume of 400 μl of chloroform was added to the homogenate. Samples were centrifuged at 17,000g for 10 min, and the resulting top layer was collected and taken to dryness under nitrogen.

Metabolomics analysis of glucose flux studies

Samples were reconstituted in 30 μl of 2:1 acetonitrile:water and filtered, and 5 μl was injected for analysis. Samples were separated as described (42). Metabolites were analyzed on the Agilent 6456 quadrupole time-of-flight mass spectrometer coupled to Agilent 1290 LC. Data were collected in negative mode, with gas temperature 225 °C, drying gas at 10 L/min, nebulizer at 40 psi, sheath gas temperature 300 °C, and sheath gas flow at 12 L/min. Fragmentor was set at 125 V, skimmer at 65 V, and VCap at 3000 V. Authentic standards of all measured metabolites were run separately and spiked into pooled samples for verification of metabolite identity and retention time.

Peroxisomal fatty acid oxidation analysis

Twenty-four-week-old *db/db* and *db/+* mice were fasted for 4 h and perfused with ice-cold PBS. Kidney cortex from mice were isolated, and approximately 20 mg of tissue was homogenized in SETH buffer (250 mM sucrose, 1 mM EDTA,

10 mM Tris-HCl [pH 7.4]) with a Dounce homogenizer on ice. $_{16}C^{13}$-palmitate conjugated to bovine serum albumin (6:1) was added as the substrate for fatty acid oxidation. Mitochondrial oxidation was inhibited with 100 μM of etomoxir. The mixture was incubated at 37 °C at 500 rpm. After 30 min, the reaction was quenched with methanol and chloroform, then centrifuged at 15,000g for 10 min at 4 °C. The resulting bottom layer was collected and taken to dryness under nitrogen. Samples were reconstituted in acetonitrile/water/isopropyl alcohol (10:5:85) and 10 mM ammonium acetate and analyzed as previously published (49) on Turbolon Spray Ion Source into an AB Sciex Triple Quadrupole/QTRAP 6500+ mass spectrometer. Monitored transitions are as follows: lauric acid (199.3 → 199.3 m/z), $_{12}C^{13}$-lauric acid (211.3 → 211.3 m/z), myristic acid (227.2 → 227.2 m/z), $_{14}C^{13}$-myristic acid (241.2 → 241.2 m/z), palmitic acid (255.2 → 255.2 m/z), and $_{16}C^{13}$-palmitic acid (271.3 → 271.3 m/z). Percent labeled $_{12}C^{13}$-lauric acid and $_{14}C^{13}$-myristic acid were calculated and normalized to kidney weight × averaged kidney weight.

Kidney biopsies processing and transcriptional profiling for the southwestern native American cohort

Kidney biopsy tissue procurement and gene expression profiling was performed as described (50, 51) on Affymetrix GeneChip Array Human Genome series U133A and Plus 2.0 (Affymetrix, Inc). Affymetrix image files were obtained, processed, normalized, and batch corrected as described (52). Briefly, manual microdissection was performed on kidney biopsies from healthy living donors and Southwestern Native Americans with T2D to extract RNA from glomerular and tubulointerstitial tissue. The study was approved by the Institutional Review Board (IRB 0000006) at the National Institute of Diabetes and Digestive and Kidney Diseases, Bethesda, Maryland, USA. All participants gave written informed consent before their participation in the study. These tissue specimens were then sent to the sequencing core and profiled on Affymetrix microarray platform. The raw data were then processed and normalized in R statistical platform using standard Affymetrix package and annotated using customCDF from Brainarray. The normalized log2 transformed expression matrix was used for all downstream analysis. Owing to ethical considerations and privacy protection, and to avoid identifying individual study participants in this vulnerable population, the Institutional Review Board of the National Institute of Diabetes and Digestive and Kidney Diseases has stipulated that individual-level gene expression and genotype data from this study cannot be made publicly available.

Immunofluorescence analysis of SIRT5 and Kmal levels in human kidney biopsies

Formalin-fixed, paraffin-embedded 2- to 3-micron sections were obtained from renal biopsies in the archives of the University of Michigan Department of Pathology. Human kidney biopsies were dewaxed, rehydrated, and subjected to heat-induced antigen retrieval by incubating in 0.1 M citrate

buffer (pH 6.0, ab93678, Abcam) using the 2100 Antigen Retriever. Endogenous peroxidase was blocked with 0.3% hydrogen peroxide (H1009, Sigma) in Tris-buffered saline (TBS, pH 7.4) for 30 min. Sections were blocked with 10% normal goat serum in 5% bovine serum albumin at room temperature for 2 h. Sections were incubated with primary antibodies, Kmal (1:150, PTM-901, PTM Biolabs) or Sirt5 (1:250, PA5-31029, Invitrogen), diluted in Da Vinci Green (PD900L, Biocare Medical) at 4 ℃ overnight. Antibody bindings were detected by using secondary antibody, Alexa Fluor 488 goat anti-rabbit IgG (green, 1:300, A11034) at room temperature for 1 h. The sections were mounted with gold antifade reagent with DAPI (P36931, Invitrogen). An Olympus DP70 Digital Microscope was used to take pictures by ×20 magnification lenses. Fluorescent signal was quantified with ImageJ.

Data analysis and statistical analysis

Quality control samples were made by pooling all the samples in the queue. These samples were run intermittently to control for machine drift and sample stability. For targeted quantitative analysis, peak areas were extracted with Agilent Mass Hunter Workstation Software Quantitative Analysis for QQQ version B.07.01. Peak areas were normalized to internal standard before quantification. For flux samples, data were processed through Agilent Profinder. Statistics were performed with GraphPad Prism 7. Data were analyzed using Student's *t* test or one-way ANOVA with Tukey's post hoc correction.

Data availability

The proteomic data that support the findings of this study are openly available at Panorama Public at https://panoramaweb.org/gvklZ4. The ProteomeXchange ID associated with the dataset is PXD037819. Accessible at: http://proteomecentral.proteomexchange.org/cgi/GetDataset?ID=PXD037819.

Author contributions—J. B., D. B. L., S. P. conceptualization; J. B., C. H., K. S., S. P. methodology; J. B. software; J. B., V. N. formal analysis; J. B., K. S., C. H., H. Z., A. I., Y. Y., V. N. investigation; W. G., J. H., R. G. N., M. K., P. S., V. N., D. B. L., S. P. resources; J. B. writing – original draft; F. C. B., W. G., R. G. N., M. K., P. S., V. N., D. B. L., S. P. writing – review & editing; J. B., V. N., K. S. visualization; S. P. supervision; J. B., S. P. funding acquisition.

Conflict of interest—The authors declare that they have no conflicts of interest with the contents of this article.

Abbreviations—The abbreviations used are: DKD, diabetic kidney disease; DMEM, Dulbecco's modified Eagle's medium; EHHADH, enoyl-CoA hydratase and 3-hydroxyacyl CoA dehydrogenase; FA, formic acid; FAO, fatty acid oxidation; FBS, fetal bovine serum; PTM, posttranslational modification; SGLT2, sodium–glucose cotransporter 2; SIRT5, sirtuin 5; T2D, type 2 diabetes; TCA, tricarboxylic acid.

References

1. Johansen, K. L., Chertow, G. M., Foley, R. N., Gilbertson, D. T., Herzog, C. A., Ishani, A., *et al.* (2021) US renal data system 2020 tnnual data report: epidemiology of kidney disease in the United States. *Am. J. Kidney Dis.* **77**, A7–A8
2. Perkovic, V., Jardine, M. J., Neal, B., Bompoint, S., Heerspink, H. J. L., Charytan, D. M., *et al.* (2019) Canagliflozin and renal outcomes in type 2 diabetes and nephropathy. *New Engl. J. Med.* **380**, 2295–2306
3. Packer, M., Anker, S. D., Butler, J., Filippatos, G., Pocock, S. J., Carson, P., *et al.* (2020) Cardiovascular and renal sutcomes with empagliflozin in heart failure. *New Engl. J. Med.* **383**, 1413–1424
4. Mosenzon, O., Wiviott, S. D., Cahn, A., Rozenberg, A., Yanuv, I., Goodrich, E. L., *et al.* (2019) Effects of dapagliflozin on development and progression of kidney disease in patients with type 2 diabetes: an analysis from the DECLARE–TIMI 58 randomised trial. *Lancet Diabetes Endocrinol.* **7**, 606–617
5. Ingelfinger, J. R., and Rosen, C. J. (2019) Clinical Credence — SGLT2 inhibitors, diabetes, and chronic kidney disease. *New Engl. J. Med.* **380**, 2371–2373
6. Forbes, J. M., and Thorburn, D. R. (2018) Mitochondrial dysfunction in diabetic kidney disease. *Nat. Rev. Nephrol.* **14**, 291–312
7. Scheijen, J. L. J. M., Hanssen, N. M. J., Waarenburg, M. P. H. van de, Jonkers, D. M. A. E., Stehouwer, C. D. A., and Schalkwijk, C. G. (2012) L(+) and D(-) lactate are increased in rlasma and urine samples of type 2 diabetes as measured by a Simultaneous quantification of L(+) and D(-) lactate by geversed-phase liquid chromatography tandem mass spectrometry. *Exp. Diabetes Res.* **2012**, 234812
8. Kim, N. H., Hyeon, J. S., Kim, N. H., Cho, A., Lee, G., Jang, S. Y., *et al.* (2018) Metabolic changes in urine and serum during progression of diabetic kidney disease in a mouse model. *Arch. Biochem. Biophys.* **646**, 90–97
9. Mora-Ortiz, M., Nuñez Ramos, P., Oregioni, A., and Claus, S. P. (2019) NMR metabolomics identifies over 60 biomarkers associated with Type II Diabetes impairment in db/db mice. *Metabolomics* **15**, 89
10. Li, M., Wang, X., Aa, J., Qin, W., Zha, W., Ge, Y., *et al.* (2013) GC/TOFMS analysis of metabolites in serum and urine reveals metabolic perturbation of TCA cycle in db/db mice involved in diabetic nephropathy. *Am. J. Physiol. Renal Physiol.* **304**, F1317–F1324
11. Sas, K. M., Kayampilly, P., Byun, J., Nair, V., Hinder, L. M., Hur, J., *et al.* (2016) Tissue-specific metabolic reprogramming drives nutrient flux in diabetic complications. *JCI Insight.* https://doi.org/10.1172/jci.insight.86976
12. Sharma, K., Karl, B., Mathew, A. V., Gangoiti, J. A., Wassel, C. L., Saito, R., *et al.* (2013) Metabolomics reveals signature of mitochondrial dysfunction in diabetic kidney disease. *J. Am. Soc. Nephrol.* **24**, 1901–1912
13. Aperia, A., Larsson, L., and Zetterstrom, R. (1981) Hormonal induction of Na-K-ATPase in developing proximal tubular cells. *Am. J. Physiol. Renal Physiol.* **241**, F356–F360

14. He, W., Newman, J. C., Wang, M. Z., Ho, L., and Verdin, E. (2012) Mitochondrial sirtuins: regulators of protein acylation and metabolism. *Trends Endocrinol. Metab.* **23**, 467–476
15. Wagner, G. R., and Hirschey, M. D. (2014) Non-enzymatic protein acylation as a carbon stress regulated by sirtuin deacylases. *Mol. Cell* **54**, 5–16
16. Imai, S., Armstrong, C. M., Kaeberlein, M., and Guarente, L. (2000) Transcriptional silencing and longevity protein Sir2 is an NAD-dependent histone deacetylase. *Nature* **403**, 795–800
17. Landry, J., Sutton, A., Tafrov, S. T., Heller, R. C., Stebbins, J., Pillus, L., *et al.* (2000) The silencing protein SIR2 and its homologs are NAD-dependent protein deacetylases. *Proc. Natl. Acad. Sci. U. S. A.* **97**, 5807–5811
18. Frye, R. A. (1999) Characterization of five human cDNAs with somology to the phosphorylationeast SIR2 gene: sir2-like proteins (sirtuins) metabolize NAD and may have protein ADP-dibosyltransferase activity. *Biochem. Biophys. Res. Commun.* **260**, 273–279
19. Galvan, D. L., Mise, K., and Danesh, F. R. (2021) Mitochondrial regulation of diabetic kidney disease. *Front. Med. (Lausanne)* **8**, 745279
20. Hirschey, M. D., and Zhao, Y. (2015) Metabolic regulation by lysine malonylation, succinylation, and alutarylation. *Mol. Cell Proteomics* **14**, 2308–2315
21. Nishida, Y., Rardin, M. J., Carrico, C., He, W., Sahu, A. K., Gut, P., *et al.* (2015) SIRT5 regulates both cytosolic and mitochondrial protein malonylation with glycolysis as a major target. *Mol. Cell* **59**, 321–332
22. Zhu, S., Batushansky, A., Jopkiewicz, A., Makosa, D., Humphries, K. M., Van Remmen, H., *et al.* (2021) Sirt5 deficiency causes tosttranslational protein malonylation and dysregulated cellular metabolism in chondrocytes under obesity conditions. *Cartilage.* https://doi.org/10.1177/1947603521993209
23. Du, Y., Cai, T., Li, T., Xue, P., Zhou, B., He, X., *et al.* (2015) Lysine malonylation is elevated in type 2 diabetic mouse models and enriched in metabolic associated proteins. *Mol. Cell Proteomics* **14**, 227–236
24. Du, Y., Hu, H., Qu, S., Wang, J., Hua, C., Zhang, J., *et al.* (2018) SIRT5 deacylates metabolism-related proteins and attenuates hepatic steatosis in ob/ob mice. *EBioMedicine* **36**, 347–357
25. Liu, H., Rosol, T. J., Sathiaseelan, R., Mann, S. N., Stout, M. B., and Zhu, S. (2021) Cellular carbon stress is a mediator of obesity-associated osteoarthritis development. *Osteoarthritis Cartilage.* https://doi.org/10.1016/j.joca.2021.04.016
26. Clark, J. Z., Chen, L., Chou, C.-L., Jung, H. J., Lee, J. W., and Knepper, M. A. (2019) Representation and relative abundance of cell-type selective markers in whole-kidney RNA-Seq data. *Kidney Int.* **95**, 787–796
27. Schilling, B., Rardin, M. J., MacLean, B. X., Zawadzka, A. M., Frewen, B. E., Cusack, M. P., *et al.* (2012) Platform-independent and label-free quantitation of proteomic data using MS1 extracted ion hhromatograms in ekyline: application to protein acetylation and phosphorylation. *Mol. Cell Proteomics* **11**, 202–214
28. Kim, J.-Y., Hickner, R. C., Cortright, R. L., Dohm, G. L., and Houmard, J. A. (2000) Lipid oxidation is reduced in obese human skeletal muscle. *Am. J. Physiol. Endocrinol. Metab.* **279**, E1039–E1044
29. Chiba, T., Peasley, K. D., Cargill, K. R., Maringer, K. V., Bharathi, S. S., Mukherjee, E., *et al.* (2019) Sirtuin 5 regulates proximal tubule fatty acid oxidation to protect against AKI. *JASN* **30**, 2384–2398
30. Portilla, D., Dai, G., Peters, J. M., Gonzalez, F. J., Crew, M. D., and Proia, A. D. (2000) Etomoxir-induced PPARα-modulated enzymes protect during acute renal failure. *Am. J. Physiol. Renal Physiol.* **278**, F667–F675
31. Park, J., Chen, Y., Tishkoff, D. X., Peng, C., Tan, M., Dai, L., *et al.* (2013) SIRT5-Mediated lysine desuccinylation impacts siverse metabolic pathways. *Mol. Cell* **50**, 919–930
32. Barbi de Moura, M., Uppala, R., Zhang, Y., Van Houten, B., and Goetzman, E. S. (2014) Overexpression of mitochondrial sirtuins wlters glycolysis and mitochondrial function in HEK293 cells. *PLoS One* **9**, e106028
33. Wiese, S., Gronemeyer, T., Ofman, R., Kunze, M., Grou, C. P., Almeida, J. A., *et al.* (2007) Proteomics iharacterization of mouse kidney peroxisomes by tandem mass spectrometry and protein correlation profiling. *Mol. Cell Proteomics* **6**, 2045–2057
34. Ranea-Robles, P., Portman, K., Bender, A., Lee, K., He, J. C., Mulholland, D. J., *et al.* (2021) Peroxisomal L-bifunctional protein (EHHADH) deficiency causes male-specific kidney hypertrophy and proximal tubular injury in mice. *Kidney360.* https://doi.org/10.34067/KID.0003772021
35. Chen, X., Tian, M., Sun, R., Zhang, M., Zhou, L., Jin, L., *et al.* (2018) SIRT5 inhibits peroxisomal ACOX1 to prevent oxidative damage and is downregulated in liver cancer. *EMBO Rep.* https://doi.org/10.15252/embr.201745124
36. Zhao, S., Xu, W., Jiang, W., Yu, W., Lin, Y., Zhang, T., *et al.* (2010) Regulation of cellular metabolism by protein lysine acetylation. *Science* **327**, 1000–1004
37. Bentley, N. L., Fiveash, C. E., Osborne, B., Quek, L.-E., Ogura, M., Inagaki, N., *et al.* (2018) Protein hypoacylation induced by Sirt5 overexpression has minimal metabolic effect in mice. *Biochem. Biophys. Res. Commun.* **503**, 1349–1355
38. Lin, J. B., Lin, J. B., Chen, H. C., Chen, T., and Apte, R. S. (2019) Combined SIRT3 and SIRT5 deletion is associated with inner retinal dysfunction in a mouse model of type 1 diabetes. *Sci. Rep.* **9**, 3799
39. Klein, K. L., Wang, M.-S., Torikai, S., Davidson, W. D., and Kurokawa, K. (1981) Substrate oxidation by isolated single nephron segments of the rat. *Kidney Int.* **20**, 29–35
40. Uchida, S., and Endou, H. (1988) Substrate specificity to maintain cellular ATP along the mouse nephron. *Am. J. Physiol. Renal Physiol.* **255**, F977–F983
41. Kang, H. M., Ahn, S. H., Choi, P., Ko, Y.-A., Han, S. H., Chinga, F., *et al.* (2015) Defective fatty acid oxidation in renal tubular epithelial cells has a key role in kidney fibrosis development. *Nat. Med.* **21**, 37–46
42. Baek, J., and Pennathur, S. (2021) Urinary 2-sydroxyglutarate rnantiomers are markedly elevated in a murine model of type 2 diabetic kidney disease. *Metabolites* **11**, 469
43. Wang, D., Luo, Y., Wang, X., Orlicky, D. J., Myakala, K., Yang, P., *et al.* (2018) The fodium-glucose botransporter 2 inhibitor dapagliflozin prevents renal and liver disease in testern diet induced obesity mice. *Int. J. Mol. Sci.* **19**, 137
44. Lan, R., Geng, H., Singha, P. K., Saikumar, P., Bottinger, E. P., Weinberg, J. M., *et al.* (2016) Mitochondrial Pathology and glycolytic phift during proximal tubule atrophy after ischemic AKI. *J. Am. Soc. Nephrol.* **27**, 3356–3367
45. Ding, H., Jiang, L., Xu, J., Bai, F., Zhou, Y., Yuan, Q., *et al.* (2017) Inhibiting aerobic glycolysis suppresses renal interstitial fibroblast activation and renal fibrosis. *Am. J. Physiol. Renal Physiol.* **313**, F561–F575
46. Li, J., Liu, H., Takagi, S., Nitta, K., Kitada, M., Srivastava, S. P., *et al.* (2020) Renal protective effects of empagliflozin *via* inhibition of EMT and aberrant glycolysis in proximal tubules. *JCI Insight* **5**, e129034
47. Yang, F., Su, H., Deng, J., Mou, L., Wang, H., Li, R., *et al.* (2021) Discovery of new human Sirtuin 5 inhibitors by mimicking glutaryl-lysine substrates. *Eur. J. Med. Chem.* **225**, 113803
48. Onorato, J. M., Chen, L., Shipkova, P., Ma, Z., Azzara, A. V., Devenny, J. J., *et al.* (2010) Liquid-liquid extraction coupled with LC/MS/MS for monitoring of malonyl-CoA in rat brain tissue. *Anal. Bioanal. Chem.* **397**, 3137–3142
49. Afshinnia, F., Rajendiran, T. M., He, C., Byun, J., Montemayor, D., Darshi, M., *et al.* (2021) Circulating free fatty acid and thospholipid nignature predicts early rapid kidney function decline in patients with type 1 diabetes. *Diabetes Care* **44**, 2098–2106
50. Schmid, H., Boucherot, A., Yasuda, Y., Henger, A., Brunner, B., Eichinger, F., *et al.* (2006) Modular activation of nuclear factor-κB Transcriptional programs in human diabetic nephropathy. *Diabetes* **55**, 2993–3003
51. Cohen, C. D., Frach, K., Schlöndorff, D., and Kretzler, M. (2002) Quantitative gene expression analysis in renal biopsies: a novel protocol for a high-throughput multicenter application. *Kidney Int.* **61**, 133–140
52. Martini, S., Nair, V., Keller, B. J., Eichinger, F., Hawkins, J. J., Randolph, A., *et al.* (2014) Integrative biology identifies shared transcriptional networks in CKD. *JASN* **25**, 2559–2572